Title
Microglia facilitate loss of perineuronal nets in the Alzheimer's disease brain

Authors
Crapser, Joshua D
Spangenberg, Elizabeth E
Barahona, Rocio A
et al.

Publication Date
2020-08-01

DOI
10.1016/j.ebiom.2020.102919

Peer reviewed

EBioMedicine 58 (2020) 102919

Contents lists available at ScienceDirect

EBioMedicine

journal homepage: www.elsevier.com/locate/ebiom

Research paper

Microglia facilitate loss of perineuronal nets in the Alzheimer's disease brain

Joshua D. Crapser, Elizabeth E. Spangenberg, Rocio A. Barahona, Miguel A. Arreola, Lindsay A. Hohsfield, Kim N. Green*

Department of Neurobiology and Behavior, University of California, Irvine, CA 92697, USA

ARTICLE INFO

Article History:
Received 19 May 2020
Revised 9 July 2020
Accepted 10 July 2020
Available online xxx

ABSTRACT

Background: Microglia, the brain's principal immune cell, are increasingly implicated in Alzheimer's disease (AD), but the molecular interfaces through which these cells contribute to amyloid beta (Aβ)-related neurodegeneration are unclear. We recently identified microglial contributions to the homeostatic and disease-associated modulation of perineuronal nets (PNNs), extracellular matrix structures that enwrap and stabilize neuronal synapses, but whether PNNs are altered in AD remains controversial.

Methods: Extensive histological analysis was performed on male and female 5xFAD mice at 4, 8, 12, and 18 months of age to assess plaque burden, microgliosis, and PNNs. Findings were validated in postmortem AD tissue. The role of neuroinflammation in PNN loss was investigated via LPS treatment, and the ability to prevent or rescue disease-related reductions in PNNs was assessed by treating 5xFAD and 3xTg-AD model mice with colony-stimulating factor 1 receptor (CSF1R) inhibitor PLX5622 to deplete microglia.

Findings: Utilizing the 5xFAD mouse model and human cortical tissue, we report that PNNs are extensively lost in AD in proportion to plaque burden. Activated microglia closely associate with and engulf damaged nets in the 5xFAD brain, and inclusions of PNN material are evident in mouse and human microglia, while aggrecan, a critical PNN component, deposits within human dense-core plaques. Disease-associated reductions in parvalbumin (PV)+ interneurons, frequently coated by PNNs, are preceded by PNN coverage and integrity impairments, and similar phenotypes are elicited in wild-type mice following microglial activation with LPS. Chronic pharmacological depletion of microglia prevents 5xFAD PNN loss, with similar results observed following depletion in aged 3xTg-AD mice, and this occurs despite plaque persistence.

Interpretation: We conclude that phenotypically altered microglia facilitate plaque-dependent PNN loss in the AD brain.

Funding: The NIH (NIA, NINDS) and the Alzheimer's Association.

1. Introduction

Alzheimer's disease (AD) is a progressive neurodegenerative disorder characterized pathologically by the accumulation of extracellular amyloid-β (Aβ) plaques and intraneuronal neurofibrillary tangles (NFTs) composed of hyperphosphorylated tau. The appearance and spread of these pathological substrates is fundamentally linked to a cascade of events that results in the synaptic dysfunction and neuronal loss characteristic of the disease, manifesting behaviorally as progressive impairments in memory and cognition [1]. Research spanning the past decade has identified numerous genes that confer increased risk of disease development [2, 3], and the majority of these risk genes are highly or solely expressed in myeloid cells (e.g. *Trem2, Cd33, Spi1, Abi3, Plcg2, Apoe*) thereby implicating microglia in AD etiology [4, 5]. In addition, genes expressed in other CNS cell types (e.g. neurons and astrocytes) have microglia-specific enhancers with risk polymorphisms that selectively affect myeloid expression (i.e. *Bin1*) [6].

Brain myeloid cells consist primarily of microglia, the resident parenchymal macrophages, and border macrophages along CNS interfaces (e.g. meningeal, perivascular, and choroid plexus macrophages) [7, 8]. As part of the glial activation characterized by Alois Alzheimer in his initial report [9], the microglial response to amyloid plaques and/or tau pathology is increasingly thought to cause or contribute heavily to disease-related neurodegeneration [10–13]. Thus, elucidating the cellular mechanisms by which microglia drive disease

* Correspondence to: Kim N. Green, Ph.D., 3208 Biological Sciences III, University of California, Irvine, Irvine, CA 92697, USA.
E-mail address: kngreen@uci.edu (K.N. Green).

https://doi.org/10.1016/j.ebiom.2020.102919

Research in context

Evidence before this study

Perineuronal nets are reticular formations of extracellular matrix that scaffold neuronal synapses, with direct involvement in neuronal plasticity and memory. The Alzheimer's disease brain is characterized by the presence of extracellular Aβ plaques, which elicit a microglia-evoked inflammatory response that is implicated in mediating subsequent synaptic and neuronal loss. However, the fate of perineuronal nets in the Alzheimer's disease brain is unclear, as well as the roles that microglia may play in regulating them.

Added value of this study

In this study, we explore the relationships between microglia, perineuronal nets, and amyloid plaques in Alzheimer's disease model and human brains through immunohistochemical analysis. We find that perineuronal nets are extensively lost in disease and identify the presence of aggrecan, a critical net component, in human dense-core plaques. We also observe close spatial association between morphologically altered perineuronal nets and disease microglia, which contain inclusions of perineuronal net material consistent with phagocytic uptake. Finally, we test the hypothesis that microglia directly contribute to perineuronal net loss via their pharmacological depletion with colony-stimulating factor 1 receptor (CSF1R) inhibitor treatment, and find that microglial depletion prevents the loss of perineuronal nets in Alzheimer's disease.

Implications of all the available evidence

Our data suggest that perineuronal net loss is a salient phenotype of the Alzheimer's disease model and human brain, and a recurring phenotype in the context of neurodegeneration overall. These results add to a growing body of research underscoring the increasingly central role microglia are believed to play in Alzheimer's disease pathogenesis by demonstrating that microglia mediate the disease-related loss of perineuronal nets. As perineuronal nets are implicated in neuronal health and function, protecting cells against neurotoxins (e.g. Aβ_{1-42}, oxidative stress) in addition to modulating neuronal activity and the synaptic landscape, the microglia-mediated loss of these structures likely plays an important role in disease outcome. Interestingly, we also show here as before that the depletion of microglia enhances basal perineuronal net levels in healthy adult mice, thereby suggesting that microglia regulate net formation in health as well as disease.

progression in the AD brain – and how this may be linked to downstream cognitive and behavioral phenotypes – is critical to understanding the disease, and in a similar vein, to the development of therapeutics that counteract these effects.

Microglia adopt a multitude of functions in the healthy and diseased CNS, and aside from immunological roles, evidence indicates that these cells interact with and modulate neuronal and synaptic elements, with direct effects on learning and memory [14–19]. The extracellular matrix (ECM), specifically the condensed ECM structure known as the perineuronal net (PNN), is an essential component of the synapse involved in the regulation of plasticity that, along with astrocytes and synaptic terminals, comprise the contemporary "tetrapartite synapse" [20]. PNNs form preferentially around fast-spiking parvalbumin (PV)+ GABAergic interneurons throughout the brain during the closure of the critical period of plasticity, effectively "locking" proximal synapses in place and providing synaptic stability [21] soon after synaptic pruning is completed by developmental microglia [22]. Although enhanced plasticity and learning is observed following experimental PNN ablation [23, 24], newly formed memory traces can interfere with the fidelity and recall of previously learned information [20], as evident by impaired reconsolidation and recall of remote memories following PNN ablation [25, 26]. Furthermore, the structural modification of PNNs alters synaptic transmission [27], synapse number [28], and the ion channel/neurotransmitter receptor composition of synapses [29], and thus may be related to the dysfunctional interneuron activity mediating cognitive impairments in AD [30, 31].

The functional capacity of microglia to remodel the ECM is classically demonstrated in acute injuries such as stroke [32], in which microglia undergo activation and subsequently release matrix metalloproteinases (e.g. MMP9) or other ECM-degrading proteases that act on PNN components [33]. However, PNN loss is also reported in other neurological disorders such as seizure [34] and prion disease [35], and recent work from our lab identified a role for microglia-mediated PNN loss in Huntington's disease [36]. Although PNNs are reported to protect neurons against tau [37, 38] and Aβ pathology [39], the extent to which PNN loss occurs in human and animal models of AD – where microglia are inextricably linked to disease pathogenesis – remains controversial [40–43].

Utilizing the aggressive 5xFAD mouse model of disease [44] and corroborated by extensive immunohistochemical (IHC) analysis of human cortical tissue, we report that PNNs are extensively lost in the mouse and human AD brain. We find that PNN deficits occur earlier in 5xFAD brain regions with high pathology, as in the subiculum, where reductions in PV+ interneuron density are observed only after impairments in regional PNN coverage and structural integrity. Activated microglia closely associate with morphologically abnormal nets in the AD brain and staining for PNN components reveals colocalization in both mouse and human microglia. Interestingly, we also find consistent colocalization of the CSPG aggrecan (ACAN) – critical to PNN structure and function [24] – with human dense-core plaques, which in turn inversely correlate with total ACAN+ PNNs across unaffected and AD brain samples. Inducing microglial activation via lipopolysaccharide (LPS) injection in wild-type (WT) mice is sufficient to cause overall PNN loss and impairments in the structural integrity of PV+ interneuron-associated PNNs, in addition to reduced PV+ cell densities. We show that chronic depletion of microglia prior to and during plaque development in 5xFAD mice with the selective colony-stimulating factor 1 receptor (CSF1R) inhibitor PLX5622 effectively prevents PNN loss, data substantiated by the similar beneficial effects on PNNs we observe with microglial depletion in aged 3xTg-AD mice. Importantly, this occurs despite the persistence of plaques. Thus, we conclude that disease-altered microglia facilitate plaque-dependent loss of PNNs in the AD mouse model and human brain.

2. Materials and methods

Compounds: PLX5622 was provided by Plexxikon Inc. and formulated in AIN-76A standard chow by Research Diets Inc. at 1200 ppm.

Mice: All animal experiments were performed according to animal protocols approved by the Institutional Animal Care and Use Committee (IACUC) at the University of California, Irvine, an American Association for Accreditation of Laboratory Animal Care (AAALAC)-accredited institution. We utilized 5xFAD mice in this study, a model of AD harboring five relevant mutations across two human transgenes, amyloid precursor protein (*APP*) and presenilin-1 (*PSEN1*), described in detail elsewhere [45] and obtained from the Mutant Mouse Resource and Research Centers (MMRRC; 034848-JAX), or 3xTg-AD mice, with three familial AD mutations (in *APP, MAPT, PSEN1*) [46]. WT mice (000664) were obtained from the Jackson Laboratory to maintain both lines on a C57BL/6J background.

Mice were housed in groups of up to five animals/cage under 12-hr light/dark cycles, with *ad libitum* access to vivarium chow and water. For timecourse experiments, naïve male and female 5xFAD and WT mice were euthanized for investigation at 4, 8, 12, and 18 months (mo). For LPS experiments, 9-month-old male and female WT mice were intraperitoneally (IP) injected with 0.5 mg/kg LPS (L4130, Sigma) or saline every other day for a week, followed by euthanasia 24hr after the last dose. To determine the role of microglia in plaque-related PNN disturbances, male and female 5xFAD and WT mice were given AIN-76A chow containing vehicle or 1200 ppm PLX5622 from 1.5 months (prior to plaque pathology) to 4 months of age. For post-pathological experiments, male and female 3xTg-AD mice were given vehicle or 1200 ppm PLX5622 orally for 1mo starting at 17mo. Assignment of animals to treatment groups was conducted in a random manner and was balanced for sex, and researchers were blinded to genotype and treatment groups during analysis of histological data.

Tissue collection:

Mouse tissue: At the end of treatment, mice were euthanized via CO2 inhalation and transcardially perfused with ice-cold 1X phosphate buffered saline. For all studies, brains were removed, and hemispheres separated along the midline. Each hemisphere was then drop-fixed in 4% paraformaldehyde (Thermo Fisher Scientific, Waltham, MA) for 48 hrs, cryoprotected in 30% sucrose + 0.05% sodium azide, and sectioned at 40 μm on a Leica SM2000R freezing microtome for immunohistochemical analysis.

Human tissue: For analysis of human brains, postmortem cortical tissue from the middle frontal gyrus (BA9 and 46) of non-demented and AD subjects was obtained from the Alzheimer's Disease Research Center (ADRC), UC Irvine. The protocols for obtaining postmortem brain tissue complied with all federal and institutional guidelines with special respect for donor identity confidentiality and informed consent. Dementia and AD diagnosis were made by a consensus conference using neuropsychological assessment, neurological examination, and medical records following DSM-IV and National Institute of Neurological and Communicative and Stroke-Alzheimer's Disease and Related Disorders Association criteria, respectively. Neuropathological examination included Braak and Braak staging for plaques and tangles and diagnosis of neuropathological AD using National Institute on Aging-Reagan criteria [47]. Neuropathological differences in non-demented (ND) control (cognitive diagnosis: ND; plaque stage: 1.67 +/- 0.24; age: 91 +/- 0.25; MMSE: 27.11 +/- 1.42) and Alzheimer's disease (AD) (cognitive diagnosis: AD; plaque stage: 3.93 +/- 0.07; age: 89.57 +/- 0.88; MMSE: 13.77 +/- 2.13) cases are listed in Table 1. Paraformaldehyde-fixed human samples were cryoprotected via 48hr incubation in 30% sucrose + 0.05% sodium azide and samples were cut into serial sections (30 μm) using a Leica SM2000R freezing microtome.

Histology and confocal microscopy: Fluorescent immunolabeling followed a standard indirect technique as described previously [13]. Brain sections were stained with antibodies against IBA1 (1:1000; 019−19741, Wako and ab5076, Abcam), *Wisteria floribunda agglutinin* (WFA) lectin (1:1000, B-1355, Vector Labs), aggrecan 7D4 (1:15, MCA1454G, Bio-Rad), aggrecan (1:200, AB1031, Millipore), CSPG CS-56 (1:200, ab11570, Abcam), and parvalbumin (1:500, MAB1572, Millipore). Thioflavin-S (Thio-S; T1892, Sigma-Aldrich) staining was performed as described before [12]. Amylo-Glo (TR-300-AG; Biosensis) staining was performed according to the manufacturer's instructions for confirmation of plaques with an additional marker where indicated. IHC was performed the same on human postmortem cortical tissue, including Thio-S pretreatment, with an additional incubation in Sudan Black B (206470; MP Biomedicals) as a final step to reduce autofluorescence. Antigen retrieval was performed prior to staining 5xFAD tissue with aggrecan (AB1031) and CSPG via 30 min incubation in pH 6.0 citric acid buffer at 80 °C, after which all IHC steps were performed normally. Immunostained sections were mounted and coverslipped with Fluoromount-G with or without DAPI (0100−20 and 0100−01; SouthernBiotech). High resolution fluorescent images were obtained using a Leica TCS SPE-II confocal microscope and LAS-X software. One 20X field-of-view (FOV) per brain region was captured per mouse, and max projections of 63X Z-stacks were used for representative images when indicated. For whole-brain stitches, automated slide scanning was performed using a ZEISS Axio Scan.Z1 equipped with a Colibri camera and ZEN Axio Scan 2.3 software.

Cell quantities were determined using the spots module in Imaris v9.2, while plaque number and PNN coverage area were determined using the surfaces module. To measure PNN structural integrity, the average value of the mean WFA fluorescence intensity within each PV+ spot (e.g. WFA+ signal colocalizing with PV+ cell body) of a particular sample was compared, adapted and modified from [48]. To measure the total WFA+ material associated with microglia, the WFA + intensity sum of each IBA1+ spot was added together for each sample. CSPG immunoreactivity was measured as integrated signal density in ImageJ (NIH) as before [36]. For the analysis of human tissue, the number of ACAN+ (aggrecan clone 7D4) PNNs and Thio-S+ dense-core plaques were manually quantified and averaged across 4 regionally distinct 20X Z-stack max projections of cortical gray matter per brain sample for $n = 9$ non-demented control and $n = 12$ AD brains to determine statistical differences. All 20X max projection values (rather than patient averages) were utilized for regression and correlation analysis, excluding any replicates in which technical artifacts were observed.

Data analysis and statistics: Statistical analysis was performed with Prism GraphPad (v.8.3.0). To compare two groups, the two-tailed unpaired Student's *t*-test was used. To compare multiple groups along one or two variables, a one-way or two-way ANOVA, respectively, was performed with Tukey's post-hoc test for multiple comparisons. All bar graphs are represented as mean ± standard error of the mean (SEM) with individual sample values overlain. Non-linear regression with Akaike's Information Criterion (AICc) was used to determine the statistical model (linear or quadratic) that best explains the data, and Pearson's or Spearman's correlation analysis was performed depending on whether the relationship was linear or nonlinear, respectively (all correlations reported in this study were nonetheless confirmed significant using both analyses). Statistical significance was accepted at $p \leq 0.05$ and is expressed as follows: $^{*}p \leq 0.05$, $^{**}p<0.01$, $^{***}p<0.001$, $^{****}p<0.0001$.

Supplementarymaterials: Fig. S1 displays the inverse relationship between WFA+ PNNs and Thio-S+ plaque burden across all timepoints (4, 8, 12, 18mo; sex-balanced) in the 5xFAD subiculum and visual cortex samples examined in Fig. 1. Fig. S2 shows WT and 5xFAD ECM CSPG accumulation at 4mo, validates WFA+ PNN loss in 5xFAD mice with aggrecan at 12mo, and demonstrates the increased

Table 1
Neuropathological differences in non-demented control (ND CON) and Alzheimer's disease (AD) cases. Values represent mean ± SEM.

Group	PMI (h)	Age (y)	Gender	MMSE	Plaque Stage	Plaque Stage (Frontal)	Tangle Stage
ND- CON	3.61 ± 0.28	91 ± 0.25	6F, 3M	27.11 ± 1.42	1.67 ± 0.24	0.33 ± 0.17	2.78 ± 0.40
AD	4.51 ± 0.39	89.57 ± 0.88	10F, 4M	13.77 ± 2.13	3.93 ± 0.07	3.00 ± 0.00	5.36 ± 0.13

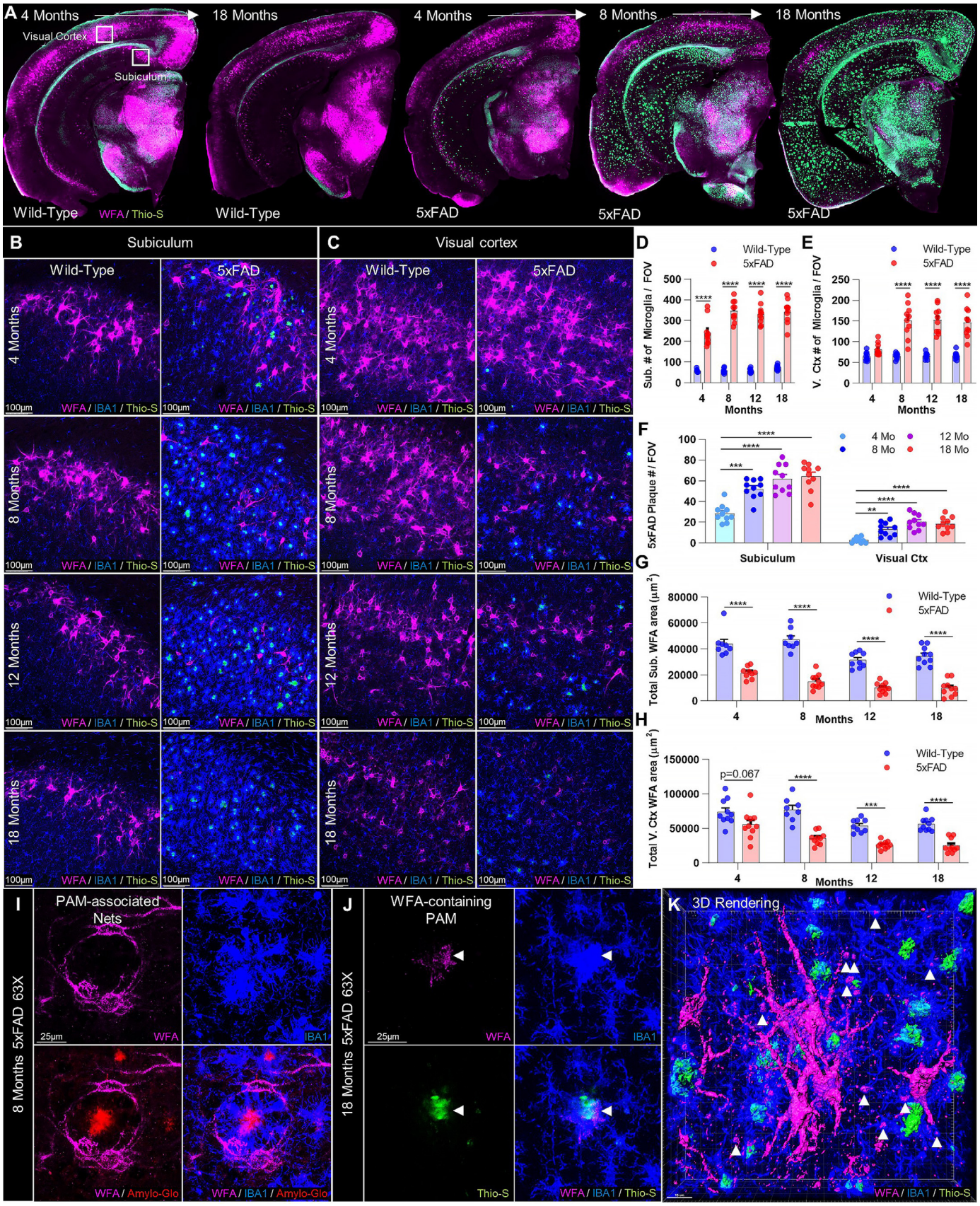

Fig. 1. Aβ plaques induce local PNN loss that expands with pathology in 5xFAD mice. (A) Representative whole-brain images of WFA+ PNNs and Thio-S+ dense-core plaques reveal extensive age- and plaque-related PNN loss in the 5xFAD brain, beginning in high pathology regions (e.g. subiculum) at 4 months (mo) and spreading globally by 18mo. **(B-C)** Representative 20X subiculum and visual cortex images display Thio-S+ plaque accumulation and IBA1+ microgliosis in spatial association with PNN abnormalities and loss at 4, 8, 12, and 18mo. **(D-E)** Microglial numbers were significantly increased compared to WT at every age in the subiculum and from 8mo on in the visual cortex (all $p<0.0001$; 2-way ANOVAs with Tukey's post-hoc test; n = 8–10/group). Age-related increases were also detected in subiculum ($p<0.0001$) and visual cortex ($p<0.0001$) between 4 and 8mo in

accumulation of WFA+ material in 5xFAD subiculum microglia at 18mo to complement the data in Fig. 1. Fig. S3 shows WT and 5xFAD PV+ cell density and colocalizing WFA+ signal intensity in the visual cortex that complements the subiculum data in Fig. 2. Fig. S4 depicts dense WFA+ debris in hippocampal CA1 that accumulates in the 5xFAD brain at later stages of disease, as in the subiculum images in Fig. 2. Movie S1 is a 3D reconstruction created with the 3D Project plugin for ImageJ displaying plaque-associated microglia (PAM) and associated PNNs in the 5xFAD brain as shown in Fig. 1 as a Z-stack max projection.

3. Results

3.1. Age- and plaque-dependent perineuronal net loss occurs in 5xFAD mouse brains

5xFAD mice serve as an aggressive mouse model of AD, displaying extensive Aβ plaque deposition and associated gliosis beginning at 3 months of age, particularly in the cortex and the subiculum of the hippocampus [44], in addition to synaptic deficits and neuronal loss at later stages of the disease [49, 45]. Microglia from these mice have been extensively characterized, revealing the canonical upregulation of disease-associated microglial markers (e.g. *Cst7, Axl, Trem2, Apoe, Ctss)* and loss of homoestatic markers (*P2ry12, Tmem119)* that reflect disease-related changes in form and function [12, 50, 51]. As before, we focused our investigation on the subiculum due to its early and aggressive plaque development, which allowed us to study the consequences of high plaque pathology in parallel with analyses of cortical regions, which display relatively lower amyloid burden at the same timepoints and in the same mice. Furthermore, we have previously conducted extensive cellular and transcriptomic characterization of these regions following CSF1R inhibitor or vehicle treatment, providing a growing biological context within which to interpret the findings of the present study [12, 13]. Therefore, to explore the effects of aging and plaque development on PNN integrity, we performed immunohistochemistry (IHC) on 5xFAD and age-matched WT control brain tissue at 4, 8, 12, and 18 months (mo) of age for dense-core plaques (Thioflavin-S (Thio-S) or Amylo-Glo), microglia (IBA1), and PNNs (WFA; Fig. 1A). PNNs were visualized as generally done by immunolabeling with *Wisteria floribunda agglutinin* (WFA) lectin, which binds component chondroitin sulfate proteoglycans (CSPGs) [33]. Examination of whole brain images revealed the characteristic presence of PNNs in multiple key regions, including the subiculum (Fig. 1B) and visual cortex (Fig. 1C).

Plaques were evident in multiple brain regions by 4mo in male and female 5xFAD mice, concomitant with the stereotypical activation and gliosis of plaque- and non-plaque-associated microglia (PAM and NPAM, respectively; Fig. 1A-C) [52, 53]. Indeed, 5xFAD mice had significantly higher microglial densities compared to WT at every timepoint in the subiculum, and from 8mo onward in the visual cortex ($p<0.0001$ in each case; Fig. 1D-E). Microglia accumulated around and near Thio-S+ plaques, which followed similar patterns of age-dependent aggregation in the two regions. Plaques were abundant in the 5xFAD subiculum at 4mo and significantly increased by 8mo ($p = 0.0002$), whereas visual cortex plaques were sparse until 8mo ($p<0.01$ vs 4mo) at which point they were evident across cortical layers, with numbers in both regions remaining stable thereafter (Fig. 1F).

Notably, we found that WFA+ PNNs were robustly decreased in 5xFAD mice, with the largest effects seen in the areas with the highest plaque number (Fig. 1A-C). This negative correlation was modeled best by a linear equation in the subiculum ($Y=-188.8*X + 23{,}957$; $r^2=0.2346$; Pearson's $r=-0.4844$, $p<0.01$; Fig. S1A), and a nonlinear quadratic equation in the visual cortex ($Y = 57{,}400 +-2383*X + 41.54*X^2$; $r^2=0.4131$; Spearman's $r=-0.6090$, $p<0.0001$; Fig. S1B) suggesting potential region-related differences. Total subiculum WFA+ area was reduced at every timepoint compared to age-matched WT mice ($p<0.0001$ in each case; Fig. 1B,G), whereas the visual cortex displayed significant losses at 8mo and every timepoint thereafter ($p<0.0001$ or $p<0.001$ in every case; Fig. 1C,H). Age-dependent PNN reductions were evident in both genotypes and regions, resulting in even greater PNN loss with disease progression in 5xFAD mice; WFA+ PNNs were significantly reduced by 12mo ($p<0.01$) and 8mo ($p<0.05$) in the diseased subiculum and visual cortex, respectively, compared to the same 5xFAD regions at 4mo, whereas significant within-genotype decreases in WT subiculum and cortical PNNs were detected later, between 8mo and 12mo ($p<0.001$, $p<0.05$).

Analysis of total extracellular CSPG with CS-56 at early stages of PNN loss, which generally labels CSPGs excluded from PNNs e.g. those found in glial scars [54, 55], revealed significant increases in the subiculum but not visual cortex ($p<0.05$, $p = 0.0818$) of 5xFAD mice (Fig. S2A-C). These results resemble the observation of CSPG in AD plaques reported almost three decades ago [56] as well as our previous findings in the context of Huntington's disease, where we observed dense CSPG accumulation in regions of PNN loss [36]. Together, this suggests that enhanced ECM CSPG deposition outside of PNNs is an underappreciated feature of neurodegeneration, and may also partially account for the beneficial effects afforded by treatment with chondroitinase ABC enzyme in AD models [57, 58] which degrades CSPGs not only found in PNNs but also in the general CNS ECM, where 98% of CNS CSPGs are found [21].

Further examination at higher magnification revealed that 5xFAD PNN-ensheathed neurites and cell bodies were observed physically wrapped around plaques, to which they appeared tethered by intermediary PAM (Fig. 1I, Movie S1). Interestingly, intracellular WFA+ material was evident in microglia (Fig. 1J-K; arrowheads), consistent with their putative phagocytic clearance. Analysis of total WFA+ intensity associated with IBA1+ microglia in the 18mo 5xFAD subiculum confirmed a significant increase compared to WT ($p<0.001$; Fig. S2G-H). Finally, disease-related effects on PNNs were validated at 12mo by staining for aggrecan, a core PNN CSPG [24], which confirmed the morphological abnormalities as well as the loss of 5xFAD subiculum and cortical PNNs at this timepoint ($p<0.001$, $p<0.05$; Fig. S2D-F). This data, together with the overlapping temporal profiles of plaque accumulation, microgliosis, and PNN density reduction, suggest that microglia facilitate the loss of PNNs in the 5xFAD brain.

3.2. Reductions in 5xFAD PV+ interneurons occur only after overt PNN loss

Impaired PV+ interneuron functioning has recently been linked to neuronal network hypersynchrony/hyperexcitability and cognitive deficits in AD [30, 31], and PV+ cell loss occurs across multiple AD models [59–62]. Given the protective and physiological benefits

5xFAD mice. **(F)** Thio-S+ plaques were substantial in the subiculum but scarce in the visual cortex at 4mo, and increased between 4 and 8mo in both subiculum and cortex ($p<0.001$, $p<0.01$; 1-way ANOVAs with Tukey's post-hoc test; $n = 10$/group), remaining at similar levels thereafter. **(G-H)** Analysis of total area coverage of WFA+ PNNs revealed significant decreases in the plaque-laden subiculum as early as 4mo with disease ($p<0.0001$) . Total WFA+ area was significantly diminished at all later timepoints compared to age-matched WT in subiculum (all $p<0.0001$) and visual cortex (8mo $p<0.0001$; 12mo $p<0.001$; 18mo $p<0.0001$). 5xFAD WFA+ area was reduced at 12 ($p<0.01$) and 18mo ($p<0.01$) in the subiculum and at 8 ($p<0.05$), 12 ($p<0.001$) and 18mo ($p<0.0001$) in the visual cortex compared to the same 5xFAD regions at 4mo. WT mice also displayed age-related decreases in WFA+ area between 8 and 12mo in both the subiculum ($p<0.001$) and the visual cortex ($p<0.05$) that did not recover by 18mo (all 2-way ANOVAs with Tukey's post-hoc test; $n = 8–10$/group). **(I)** Representative 63X image displays WFA+ PNNs physically wrapped around an Amylo-Glo+ plaque by intermediary plaque-associated microglia (PAM) at 8mo, commonly seen in the 5xFAD brain. **(J)** Representative 63X image and **(K)** 3D rendering of WFA+ components observable within 5xFAD microglia (arrowheads; primarily in PAM) at 18 months. Statistical significance is denoted by * $p \leq 0.05$, ** $p<0.01$, *** $p<0.001$, **** $p<0.0001$, ns = not significant. Error bars indicate SEM.

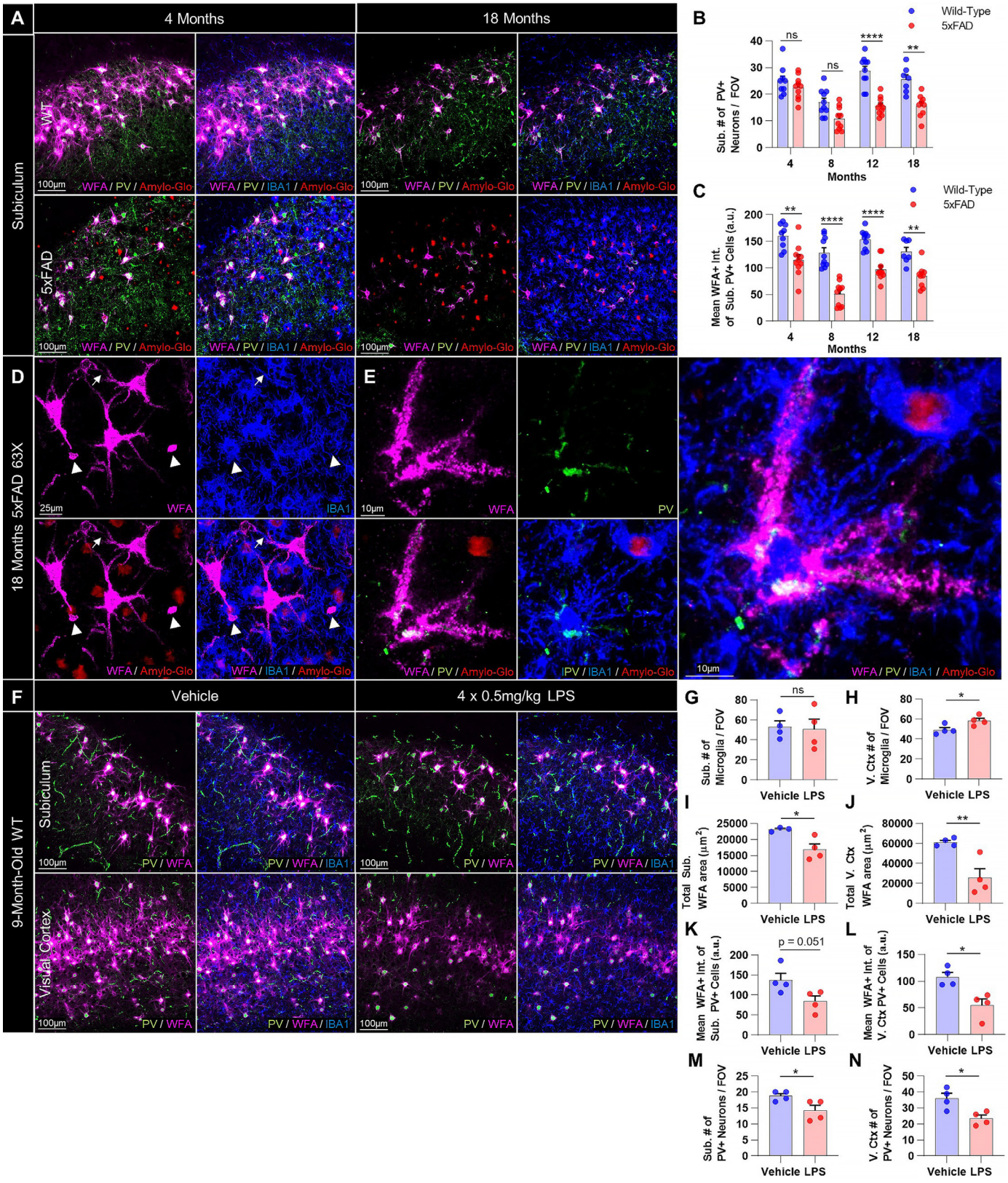

Fig. 2. PV+ interneurons are decreased following PNN loss in 5xFAD mice and these effects are mirrored by LPS-induced microglial activation. (A) Representative 20X images of WT and 5xFAD subiculum at 4 and 18 months stained for WFA, PV, IBA1, and Amylo-Glo show a loss of PNN-associated PV+ interneurons at later stages of disease. **(B)** Quantification of PV+ interneurons in 5xFAD subiculum revealed significant reductions in cell density at 12 ($p<0.0001$) and 18mo ($p<0.01$) compared to age-matched controls, and significant within-genotype decreases between 4 and 18mo in 5xFAD mice ($p<0.05$; 2-way ANOVA with Tukey's post-hoc test; n = 7–10 WT and 9–10 5xFAD/timepoint). **(C)** Mean intensity of WFA+ signal colocalizing with PV+ cell soma, a measure of structural PNN integrity, was significantly reduced in existing PV+ cells at every timepoint examined in 5xFAD subiculum (4mo $p<0.01$; 8mo $p<0.0001$; 12mo $p<0.0001$; 18mo $p<0.01$; 2-way ANOVA with Tukey's post-hoc test; n = 7–10 WT and 9–10 5xFAD/timepoint). **(D)** Representative 63X image of 18mo 5xFAD subiculum displays the condensed, debris-like WFA+ puncta (arrowheads; also see Fig. S4) that accumulate around microglia as PNN degradation progresses in late stages of disease, particularly abundant in the hippocampus but also evident in other regions (e.g. cortex). Notably, microglial process coverage of PNN-enwrapped neurites

PNNs confer upon the neurons they enwrap [39, 63], we set out to investigate the temporal pattern of PV+ interneuron loss reported in the 5xFAD brain [59, 64] relative to the onset of overt PNN reductions. To accomplish this, we immunolabeled and quantified PV+ cell density at 4, 8, 12, and 18mo in male and female 5xFAD and WT subiculum (Fig. 2A) and at 4mo and 18mo in the cortex (Fig. S3). Interestingly, PV+ cell numbers remained unchanged at 4mo and 8mo in the 5xFAD subiculum (p = 0.085 at 8mo; Fig. 2B), when PNN loss is already extensive, but were significantly reduced at 12mo and 18mo compared to WT ($p<0.0001$, $p<0.01$) and to 5xFAD at 4mo ($p<0.05$, $p<0.05$), indicating that interneurons are included among the general neuronal loss that we and others have reported in the diseased subiculum [13, 44]. Mean intensity of WFA+ signal colocalizing with subiculum PV+ neurons, a measure of the structural integrity of interneuron-associated PNNs, was significantly reduced at every age compared to WT ($p<0.01$, $p<0.0001$, $p<0.0001$, $p<0.01$ starting at 4mo; Fig. 2C), indicating that PV+ PNN component density and/or integrity is diminished prior to PV+ neuronal loss, and remains impaired in surviving cells at later ages. This trajectory of PNN impairment (in overall coverage and in PV+ cell-associated signal) prior to PV+ cell loss is consistent with reports in the hippocampus of the Tg2576 AD model [41] and with the protective properties of PNNs against AD-relevant neurotoxins (e.g. oxidative stress, Aβ) [39, 65], which when lost likely render neurons more susceptible to pathology-related death. We were unable to detect any disease-related differences in PV+ cell density in the anterior visual cortex at 4mo or 18mo, although some loss in PV+ neuronal WFA+ intensity was evident (Fig. S3A-C).

Interestingly, small debris-like WFA+ puncta, phenotypically distinct from PNNs, were abundant throughout the 5xFAD brain by 18mo, particularly in the hippocampus (e.g. subiculum, CA1) where they associated with PAM (Fig. 2D; arrowheads) and NPAM (Fig. S4A; arrowheads). Gross morphological deficits in PNNs and PV+ neurons were apparent proximal to activated (e.g. amoeboid) microglia, often suggestive in appearance of microglial-mediated disruption and/or engulfment of PV+ soma and encapsulating PNN (Fig. 2E). To determine whether microglial activation in an established model of neuroinflammation was sufficient to induce PNN degradation, adult male and female WT mice were I.P. injected at 9mo with 0.5 mg/kg LPS every other day for 7d (4 doses total) and their brains immunolabeled for PV, WFA, and IBA1 (Fig. 2F) [14]. LPS induced phenotypic activation of subiculum and cortical microglia (e.g. process retraction and enlargement), and while IBA1+ numbers were significantly elevated only in the latter ($p<0.05$; Fig. 2G-H), WFA+ area was significantly reduced in both regions ($p<0.05$, $p<0.01$; Fig. 2I-J) with reductions in mean WFA+ intensity of PV+ neurons (p = 0.051, $p<0.05$; Fig. 2K-L) and PV+ cell densities ($p<0.05$, $p<0.05$; Fig. 2M-N) resembling that seen in 5xFAD mice. Together, these data suggest that microglial activation or dyshomeostasis (induced by plaques or LPS) can result in PNN breakdown, potentially leaving interneurons and other PNN-associated subtypes susceptible to changes in synaptic connectivity [20], excitability [63], firing rate [66], and damage [39].

3.3. PNNs are reduced in human AD brains and are inversely related to plaque burden

The vulnerability of PNNs to AD pathology in humans is unclear, with some groups reporting no changes [42, 43, 67] and others reporting disease-associated reductions [40, 68]; such ambiguity may be due in part to differences in quantitative technique, disease stage/pathology progression, or regional variability. As prolonged postmortem delay (PMD, or postmortem interval, PMI) between death and tissue collection/fixation has been shown to reduce reactivity for WFA lectin in mice, but not for the major PNN component aggrecan (using pan-aggrecan clone 7D4 [69]), it has been suggested that early lectin binding site loss due to PMD may lead to discrepancies upon autopsy [42]. A recent report furthermore found clone 7D4 to be uniquely efficacious in staining PNNs in banked postmortem human middle frontal gyrus and hippocampal brain tissue, even among other aggrecan antibodies and where WFA had failed [70]. Therefore, we immunolabeled postmortem cortical tissue from clinically and neuropathologically diagnosed AD and non-demented control brains for ACAN+ PNNs (aggrecan 7D4), dense-core plaques (Thio-S), and microglia (IBA1+) (Fig. 3A-D). As in the animal studies, we included only dense-core plaques in our analysis, meaning plaques composed of a central amyloid core surrounded by a fibrillar "halo" [71, 72], due to the unique association and response of microglia to dense-core rather than diffuse plaques [12, 73–75]. Neuropathological scoring of postmortem samples can be found in Table 1.

We found that AD patient brains exhibited significantly fewer PNNs ($p<0.01$; Fig. 3E) and more Thio-S+ dense-core plaques ($p<0.001$; Fig. 3F) compared to non-demented control brains, such that a highly significant negative correlation between ACAN+ PNNs and Thio-S+ plaques was observed across unaffected and diseased tissue samples (Spearman's $r=-0.49$, $p<0.0001$; Fig. 3G). Interestingly, these data were best described by a nonlinear quadratic model ($Y = 13.91+-5.414*X + 0.7059*X^2$; $r^2=0.2094$), as paralleled by the distribution of WFA+ PNN area vs. Thio-S+ plaque number in the murine cortex but not subiculum (Fig. S1B,A), providing additional cross-species corroboration on the brain-region dependent relationship between PNNs and plaques. PAM were readily evident around dense-core plaques (Fig. 3D, arrows), and closer examination revealed the ubiquitous presence of aggrecan within both the plaque core and surrounding microglia (Fig. 3H), the processes of which could be seen in close spatial association with nearby intact PNNs (Fig. 3I).

3.4. Microglia facilitate plaque-dependent loss of PNNs

Given the relationships between plaques, microglia, and PNNs, the physical associations between NPAMs/PAMs and PNNs, and the observation that LPS also induces microglial activation and PNN degradation, we set out to directly test the involvement of microglia-mediated PNN loss in two AD mouse models. Microglia express and are critically dependent upon signaling through the myeloid CSF1/IL-34 receptor CSF1R for survival [14]. In recent years, we have developed microglial depletion paradigms based on oral delivery of CSF1R inhibitors in chow at concentrations that cross the blood-brain barrier, inducing scalable microglial death and sustained depletion from the brain [14, 76], including in mouse models of AD [12, 13, 77]. Thus, to elucidate the role of microglia in plaque-induced PNN degradation, we treated WT and 5xFAD mice with the selective CSF1R inhibitor PLX5622 (1200 ppm in chow) or vehicle from 1.5 – 4 months of age, encompassing the period in which plaques begin to form and cause PNN loss. Brain sections collected from 4mo mice at the end of the experiment were stained with Thio-S, IBA1, and WFA, and the

is extensive in regions of lower WFA+ intensity (arrows). **(E)** Representative 63X image of morphologically dystrophic PV+ interneuron and associated PNN in spatial relation to activated microglia in 18mo 5xFAD CA1 shows direct contact. **(F)** Representative 20X images of adult WT subiculum and visual cortex from mice given IP injections of saline or LPS every other day for 7 days (4 doses) demonstrating microglia-mediated neuroinflammation and consequent loss of PNNs and PV+ cell density. **(G-H)** Microglia were increased in number in the visual cortex ($p<0.05$; two-tailed unpaired t-test; n = 4/group) and displayed morphological hallmarks of activation in both subiculum and cortex. **(I-J)** LPS induced significant decreases in WFA+ coverage in the subiculum ($p<0.05$) and visual cortex of adult WT mice ($p<0.01$; two-tailed unpaired t-test; n = 3–4/group), **(K-L)** diminished WFA+ signal intensity of subiculum and visual cortex PV+ neurons (p = 0.051, $p<0.05$; two-tailed unpaired t-test; n = 4/group), and **(M-N)** reduced PV+ cell densities in both regions ($p<0.05$, $p<0.05$; two-tailed unpaired t-test; n = 4/group). Statistical significance is denoted by * $p \leq 0.05$, ** $p<0.01$, *** $p<0.001$, **** $p<0.0001$, ns = not significant. Error bars indicate SEM.

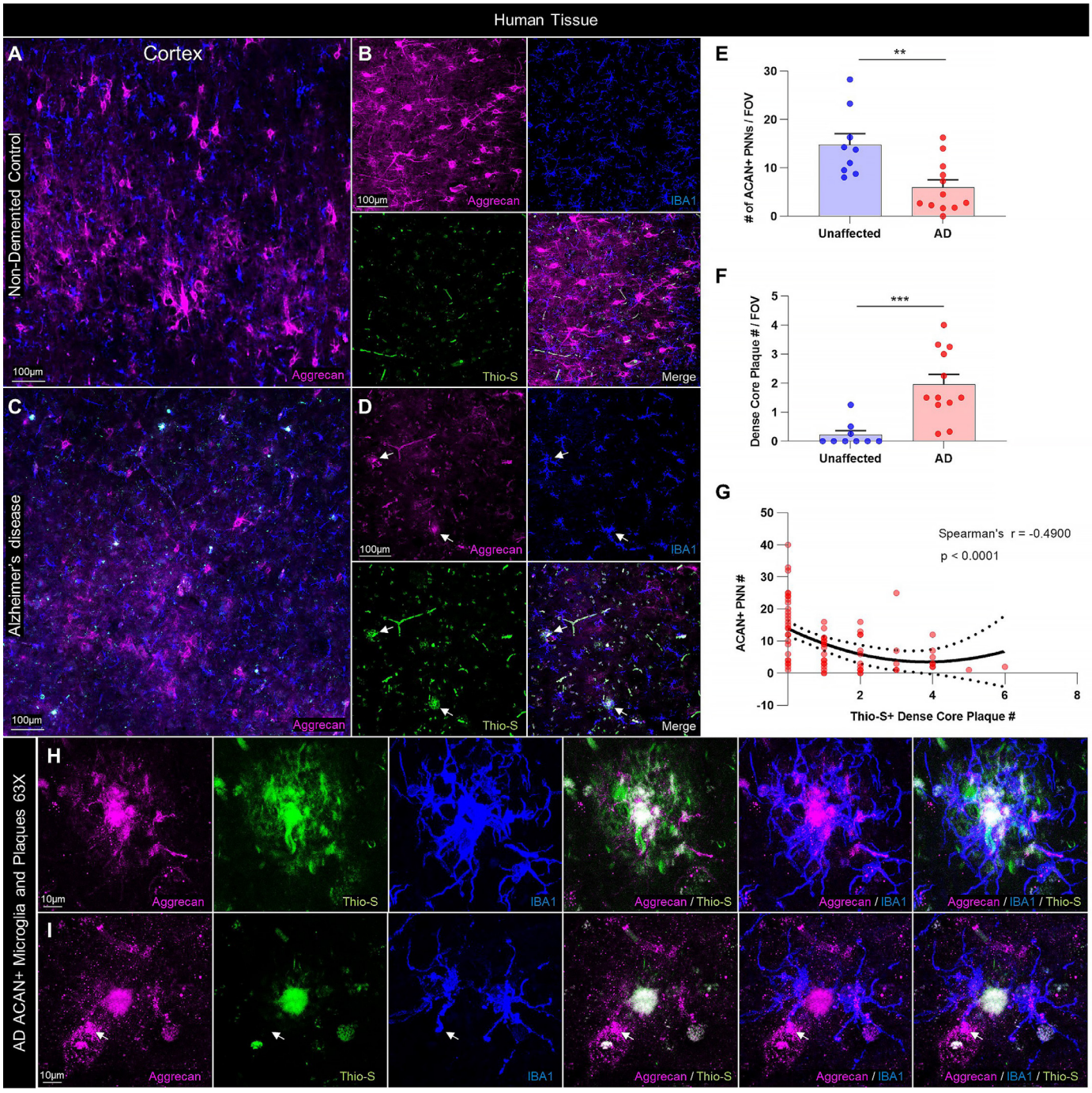

Fig. 3. PNNs are reduced in the human AD cortex and correlate negatively with dense-core plaque load. (A-B) Representative stitched and 20X images of gray matter (GM) aggrecan (ACAN)+ PNNs immunolabeled in postmortem cortical tissue from the middle frontal gyrus (BA9 and BA46) of non-demented control or **(C-D)** clinically diagnosed AD patients reveals substantial PNN loss in the diseased brain, where Thio-S+ dense-core plaques (arrows) and immediately proximal IBA1+ PAMs accumulate. **(E)** Quantification of ACAN+ PNN number in sections from $n = 9$ non-demented control and $n = 12$ AD brains revealed a significant loss with disease ($p<0.01$; two-tailed unpaired t-test; $n = 9–12$/group) in parallel with **(F)** a significant increase in Thio-S+ dense core plaques in AD compared to non-demented control brains ($p<0.001$; two-tailed unpaired t-test; $n = 9–12$/group). **(G)** Nonlinear regression and correlational analysis of human PNN and dense-core plaque counts across all sample replicates from AD and non-demented control brains identified a nonlinear ($Y = 13.91+–5.414*X + 0.7059*X^2$; $r^2=0.2094$) and highly significant inverse relationship between PNNs and plaque count in human prefrontal cortex GM (Spearman's $r=–0.49$, $p<0.0001$; $n = 80$). **(H-I)** Representative 63X images of AD patient cortical GM displays colocalization of ACAN+ signal (clone 7D4) within Thio-S+ plaques and IBA1+ microglia, suggesting the presence of PNN material. As in 5xFAD mice, PAM processes were seen in contact with proximal PNNs, occasionally with morphology resembling phagocytic cups (arrow). Statistical significance is denoted by * $p \leq 0.05$, ** $p<0.01$, *** $p<0.001$, **** $p<0.0001$, ns = not significant. Error bars indicate SEM.

relationships between plaques, microglia, and PNNs were explored (Fig. 4A, B).

Significant reductions in PNN area were evident in vehicle-treated 5xFAD subiculum compared to vehicle-treated WT at 4 months ($p<0.01$), as previously observed. However, PLX5622 completely prevented the loss of 5xFAD PNNs ($p<0.05$), which were consequently no different from vehicle-treated WT levels ($p = 0.884$; Fig. 4C). In this cohort, we detected a significant reduction in 5xFAD visual cortex WFA+ coverage at 4mo compared to vehicle-treated WT ($p<0.01$), which was also prevented in 5xFAD+PLX5622 tissue ($p<0.001$) where PNN abundance was indistinguishable from WT controls ($p = 0.827$; Fig. 4D). Importantly, the preservation of PNNs in

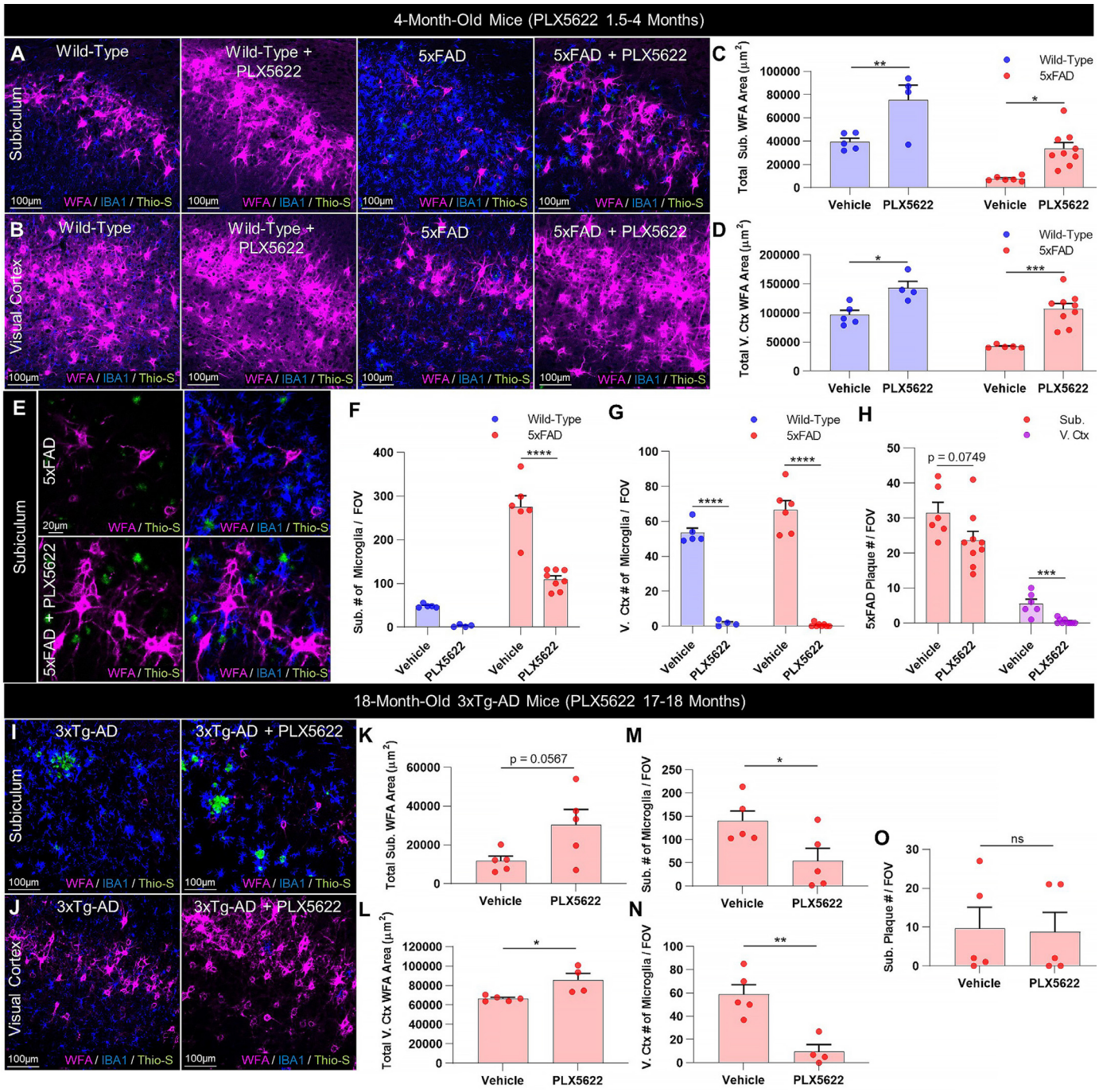

Fig. 4. Microglia mediate plaque-driven PNN loss in AD. (A-B) Representative 20X images of subiculum and visual cortex in 4mo 5xFAD and WT mice treated prior to and during plaque development (1.5–4mo) with sustained delivery of CSF1R inhibitor PLX5622 (1200 ppm in chow) demonstrate complete prevention of WFA+ PNN loss with microglial depletion in 5xFAD subiculum and cortex, even despite the persistence of Thio-S+ plaques in the former. **(C-D)** Quantification of WFA+ area in vehicle-treated mice revealed a significant decrease in 4mo 5xFAD subiculum ($p<0.01$) and visual cortex ($p<0.01$) in this cohort , both of which were prevented with PLX5622 treatment (Subiculum: 5xFAD vs. 5xFAD +PLX5622, $p<0.05$; WT vs. 5xFAD+PLX5622, $p = 0.884$. Visual cortex: 5xFAD vs. 5xFAD+PLX5622, $p<0.001$; WT vs 5xFAD+PLX5622, $p = 0.827$; all 2-way ANOVAs with Tukey's post-hoc test; $n = 4–5$ WT and 5–9 5xFAD/group). **(E)** Representative scaled 20X images and **(F)** quantification of IBA1+ microglia in vehicle- and PLX5622-treated 5xFAD subiculum confirm significant microglial depletion with treatment in diseased mice ($p<0.0001$) with predominantly PAM remaining, whereas microglia were elevated in vehicle-treated 5xFAD subiculum compared to control ($p<0.0001$; 2-way ANOVA with Tukey's post-hoc test; $n = 4–5$ WT and 6–8 5xFAD/group). **(G)** Visual cortex microglia were significantly elevated at 4mo in vehicle-treated 5xFAD compared to WT ($p<0.05$) but were virtually absent following PLX5622 ($p<0.0001$; 2-way ANOVA with Tukey's post-hoc test; $n = 4–5$ WT and 6–8 5xFAD/group). **(H)** PLX5622 significantly reduced Thio-S+ plaque numbers in the visual cortex ($p<0.001$) but not subiculum ($p = 0.0749$; two-tailed unpaired t-tests; $n = 6–9$/group), together suggesting that microglial depletion can prevent PNN loss even without significant changes in plaque load. **(I-J)** Representative 20X images of aged 18mo 3xTg-AD subiculum and visual cortex following 1mo treatment with PLX5622 (1200 ppm in chow) display beneficial effects of post-pathological IBA1+ microglial depletion on WFA+ PNNs independent of Thio-S+ plaque burden. **(K-L)** Quantification of WFA+ area reveals significant increases in subiculum and visual cortex PNNs ($p = 0.0567$, $p<0.05$) following 1-month PLX5622, which **(M-N)** significantly reduced microglia in the respective regions ($p<0.05$, $p<0.01$) but **(O)** had no effect on plaque number (subiculum $p = 0.917$; two-tailed unpaired t-tests; $n = 4–5$/group). No plaques were detected in any 3xTg-AD visual cortex images examined regardless of treatment. Statistical significance is denoted by * $p \leq 0.05$, ** $p<0.01$, *** $p<0.001$, **** $p<0.0001$, ns = not significant. Error bars indicate SEM.

the 5xFAD brain with PLX5622 coincided with extensive microglial depletion in both the subiculum ($p<0.0001$) and visual cortex ($p<0.0001$) compared to respective vehicle-treated 5xFAD regions (Fig. 4F-G). However, only Thio-S+ plaques in the visual cortex were significantly reduced with treatment ($p<0.001$; Fig. 4H), consistent with prior data [12]. A small population of mostly PAM remained in the subiculum, a region of high pathology, at 4mo following sustained CSF1R inhibition, but the reduction in overall microglial densities with PLX5622 fully preserved subiculum PNNs despite partial contact with surviving PAM (Fig. 4E). Significant microgliosis occurred alongside disease-related PNN loss in vehicle-treated 5xFAD subiculum ($p<0.0001$) and cortex ($p<0.05$) compared to vehicle-treated WT (Fig. 4F-G). PLX5622 treatment in WT mice also enhanced basal PNN levels in subiculum ($p<0.01$) and cortex ($p<0.05$) compared to vehicle treatment (Fig. 4C-D), consistent with our prior reports of homeostatic PNN regulation by microglia in the healthy adult brain [36].

To expand upon this data and to determine if microglia-mediated PNN loss could be ameliorated in late stages of disease, we treated 17mo 3xTg-AD mice, an AD line that develops clinically-relevant neurofibrillary tangles of hyperphosphorylated tau in addition to Aβ plaques [78], for 1mo with PLX5622 (1200 ppm in chow). PLX5622 treatment in 3xTg-AD mice induced extensive IBA1+ microglial depletion (subiculum $p<0.05$; visual cortex $p<0.01$) but no changes in Thio-S+ plaques (subiculum $p = 0.917$; visual cortex had no detectable plaques). Nonetheless, treatment was accompanied by significant WFA+ PNN upregulation (subiculum $p = 0.0567$; visual cortex $p<0.05$; Fig. 4I-O). Together, this data collectively suggests that the deleterious effects of AD-associated plaques on PNNs are mediated by microglia, the pre- or post-pathological depletion of which mitigates perineuronal net loss even in the absence of significant changes in plaque load.

4. Discussion

In conclusion, our data show that microglia are critical homeostatic regulators of PNNs in the healthy adult brain, and that their phenotypic changes in response to plaques mediate extensive PNN loss in AD. We observed PNN components within microglia in both mice and humans, suggesting that microglia phagocytose these ECM structures directly or the debris resulting from their degradation (e.g. following enzymatic breakdown), as well as within human dense-core plaques. The inversely correlative relationship between plaques and PNNs in the human cortex suggests that degraded PNN components may accumulate in plaques following PNN loss as AD progresses. As PNNs are implicated in neuronal health and function, protecting cells against neurotoxins such as Aβ_{1-42} [39] and oxidative stress [65] in addition to modulating neuronal activity [63, 66], the microglia-mediated loss of these structures in disease likely plays an important role in AD pathogenesis.

For instance, synaptic loss is a key feature of AD pathogenesis mediated, at least in part, by microglia [13, 79]. This may be due in part to the degradation of the PNNs in which synapses are embedded, as the genetic ablation of one or more PNN structural components and consequent loss of neuronal PNN integrity can induce the loss of synapses [28, 80] and impaired synaptic colocalization/expression of neurotransmitter receptor subunits [29], potentially manifesting as deficits in synaptic plasticity (e.g. LTP) [81–83]. We previously reported that neuronal and synaptic genes (e.g. *Dlk2, Kcnq3, Nrg3, Scn1b*) and related functional pathways (e.g. synaptic vesicles, glutamate receptors, neuronal membranes) were extensively and uniquely downregulated in the 7mo 5xFAD hippocampus compared to WT hippocampus and other 5xFAD brain regions [12], respectively, in addition to a loss of subiculum neurons and dendritic spines in 10-month-old 5xFAD mice [13]. We now know that these transcriptional and cellular alterations indicative of impaired plasticity occur alongside contemporaneous PNN loss in the subiculum, and as microglial depletion was able to prevent or rescue the regional deficits in neuronal form and function in both prior studies, we are inclined to speculate that microglia-mediated PNN loss underlies at least aspects of impaired neuronal plasticity in 5xFAD mice.

Of further relevance to AD, the enzymatic degradation of auditory cortex PNNs with chondroitinase ABC (chABC) disrupts consolidation of auditory fear learning [84], which is restored upon PNN recovery, whereas PNN digestion in the amygdala or visual cortex disrupts the recall of contextual fear memories [85] and remote visual fear memories [26], respectively. Similarly, PNN formation in the hippocampus is required for the consolidation and reconsolidation of recent and remote fear memories [25]. In light of such data, PNNs have been proposed as the molecular substrate underpinning long-term memory storage, by serving as a scaffold that retains synapse position and strength [86]. Although contrasting effects of PNN ablation on certain (specifically object recognition) memory tasks and measures of plasticity suggest this is not the case for all types of memory [21, 29, 87], such differences may also be at least partly attributable to the PNN ablation method utilized (e.g. enzymatic digestion vs genetic deletion of PNN components) which can produce differential effects on the same measures of plasticity [82]. On the other hand, enhanced plasticity and learning can impair the storage and recall of remote memories due to interference from new memory traces [20], and so the enhancement of these factors following PNN loss would still be consistent with the consequently impaired reconsolidation and recall of remote, long-term memories reported by others [25, 26]. Supporting this, a recent study found that while PNN digestion enhanced learning rate, it ultimately impaired memory retention, due in part to the extensive synaptic remodeling induced by PNN loss [88].

It is interesting to note that we identified here and elsewhere [36] a homeostatic role for microglia in the maintenance of PNNs, such that basal PNN levels in the healthy adult brain are elevated following microglial depletion. Recent work in mice shows that microglial clearance of ECM in response to neuronal IL-33 promotes synaptic remodeling and plasticity [89]. Importantly, inhibiting this pathway results in reduced microglial phagocytosis and engulfment of ECM components (e.g. aggrecan) and conversely enhanced deposition of ECM at synapses [89], and therefore the consequences of this loss of microglial function resemble the enhanced accumulation of ECM-composed PNNs that we have shown occurs in healthy adult mice following the pharmacological loss of microglia themselves [36]. Microglial depletion also enhances performance in certain memory tasks [12, 14, 16] and prevents the forgetting of remote memories, and in association, the dissociation of memory engram cells in healthy adult mice [18]. While further research is necessary to unweave the complexities and mechanisms of PNN modulation by microglia and specifically how this relates to changes in synapses and memory, the occurrence of microglia-mediated PNN loss, which we first reported in the Huntington's disease brain even in the absence of overt microglial activation [36], and now extend to the AD brain, suggests that ECM remodeling by glia is a common feature of neurodegenerative disorders. Identifying therapeutic avenues that inhibit microglia-mediated PNN loss without requiring their cellular ablation will be critical going forward.

Author contributions

J.D.C. conceived and performed experiments, analyzed data, and wrote the manuscript. E.E.S., R.A.B., and M.A.A. performed experiments. L.A.H. edited the manuscript and provided feedback. K.N.G. conceived experiments, wrote the manuscript, provided supervision, and secured funding.

Acknowledgments

This work was supported by the National Institutes of Health (NIH) under awards: R01NS083801 (NINDS), R01AG056768 (NIA), and P50AG016573 (NIA), and U54 AG054349 (NIA Model Organism Development and Evaluation for Late-onset Alzheimer's Disease (MODEL-AD)) to K.N.G., F31NS108611 (NINDS) to J.D.C., F31AG059367 (NIA) and T32AG00096 (NIA) to E.E.S., F31NS111882 (NINDS) to M.A.A., and AARF-16–442762 (Alzheimer's Association) to L.A.H. The content is solely the responsibility of the authors and does not necessarily represent the official views of the National Institutes of Health. Sources of funding did not have any role in study design, data collection or analysis, interpretation of results, or manuscript preparation or submission. We thank Edna Hingco for her excellent technical assistance, and Brian L. West and Andrew Rymar at Plexxikon, Inc. for providing and formulating CSF1R inhibitor chow. The authors declare no competing financial interests.

Supplementary materials

Supplementary material associated with this article can be found, in the online version, at doi:10.1016/j.ebiom.2020.102919.

References

[1] Selkoe DJ, Hardy J. The amyloid hypothesis of Alzheimer's disease at 25 years. EMBO Mol Med 2016;8:595–608.
[2] Karch CM, Jeng AT, Nowotny P, Cady J, Cruchaga C, Goate AM. Expression of novel Alzheimer's disease risk genes in control and Alzheimer's disease brains. PLoS ONE 2012;7:e50976.
[3] Van Cauwenberghe C, Van Broeckhoven C, Sleegers K. The genetic landscape of Alzheimer disease: clinical implications and perspectives. Genetics in Medicine 2016;18:421–30.
[4] Sierksma, A., Lu, A., Mancuso, R., Fattorelli, N., Thrupp, N., Salta, E., Zoco, J., Blum, D., Buée, L., De Strooper, B., et al. Novel Alzheimer risk genes determine the microglia response to amyloid-β but not to TAU pathology. EMBO Mol Med*n/a*, e10606.
[5] Sims R, van der Lee SJ, Naj AC, Bellenguez C, Badarinarayan N, Jakobsdottir J, Kunkle BW, Boland A, Raybould R, Bis JC, et al. Rare coding variants in PLCG2, ABI3, and TREM2 implicate microglial-mediated innate immunity in Alzheimer's disease. Nat. Genet. 2017;49:1373–84.
[6] Nott A, Holtman IR, Coufal NG, Schlachetzki JCM, Yu M, Hu R, Han CZ, Pena M, Xiao J, Wu Y, et al. Brain cell type–specific enhancer–promoter interactome maps and disease-risk association. Science 2019;366:1134–9.
[7] Kierdorf K, Prinz M. Microglia in steady state. J. Clin. Invest. 2017;127:3201–9.
[8] Li Q, Barres BA. Microglia and macrophages in brain homeostasis and disease. Nature reviews Immunology 2018;18:225–42.
[9] Stelzmann RA, Norman Schnitzlein H, Reed Murtagh F. An english translation of alzheimer's 1907 paper, "über eine eigenartige erkankung der hirnrinde". Clinical Anatomy 1995;8:429–31.
[10] Krasemann S, Madore C, Cialic R, Baufeld C, Calcagno N, El Fatimy R, Beckers L, O'Loughlin E, Xu Y, Fanek Z, et al. The TREM2-APOE Pathway Drives the Transcriptional Phenotype of Dysfunctional Microglia in Neurodegenerative Diseases. Immunity 2017;47:566–81 e569.
[11] Shi Y, Manis M, Long J, Wang K, Sullivan PM, Remolina Serrano J, Hoyle R, Holtzman DM. Microglia drive APOE-dependent neurodegeneration in a tauopathy mouse model. J. Exp. Med. 2019;216:2546–61.
[12] Spangenberg E, Severson PL, Hohsfield LA, Crapser J, Zhang J, Burton EA, Zhang Y, Spevak W, Lin J, Phan NY, et al. Sustained microglial depletion with CSF1R inhibitor impairs parenchymal plaque development in an Alzheimer's disease model. Nat Commun 2019;10:3758.
[13] Spangenberg EE, Lee RJ, Najafi AR, Rice RA, Elmore MR, Blurton-Jones M, West BL, Green KN. Eliminating microglia in Alzheimer's mice prevents neuronal loss without modulating amyloid-beta pathology. Brain 2016;139:1265–81.
[14] Elmore MR, Najafi AR, Koike MA, Dagher NN, Spangenberg EE, Rice RA, Kitazawa M, Matusow B, Nguyen H, West BL, et al. Colony-stimulating factor 1 receptor signaling is necessary for microglia viability, unmasking a microglia progenitor cell in the adult brain. Neuron 2014;82:380–97.
[15] Elmore MRP, Hohsfield LA, Kramár EA, Soreq L, Lee RJ, Pham ST, Najafi AR, Spangenberg EE, Wood MA, West BL, et al. Replacement of microglia in the aged brain reverses cognitive, synaptic, and neuronal deficits in mice. Aging Cell 2018;17:e12832.
[16] Rice RA, Spangenberg EE, Yamate-Morgan H, Lee RJ, Arora RP, Hernandez MX, Tenner AJ, West BL, Green KN. Elimination of Microglia Improves Functional Outcomes Following Extensive Neuronal Loss in the Hippocampus. J. Neurosci. 2015;35:9977–89.
[17] Tremblay M, Stevens B, Sierra A, Wake H, Bessis A, Nimmerjahn A. The role of microglia in the healthy brain. J. Neurosci. 2011;31:16064–9.
[18] Wang C, Yue H, Hu Z, Shen Y, Ma J, Li J, Wang X-D, Wang L, Sun B, Shi P, et al. Microglia mediate forgetting via complement-dependent synaptic elimination. Science 2020;367:688–94.
[19] Werneburg S, Jung J, Kunjamma RB, Ha S-K, Luciano NJ, Willis CM, Gao G, Biscola NP, Havton LA, Crocker SJ, et al. Targeted Complement Inhibition at Synapses Prevents Microglial Synaptic Engulfment and Synapse Loss in Demyelinating Disease. Immunity 2020;52:167–82 e167.
[20] Reichelt AC, Hare DJ, Bussey TJ, Saksida LM. Perineuronal Nets: plasticity, Protection, and Therapeutic Potential. Trends Neurosci. 2019;42:458–70.
[21] Fawcett JW, Oohashi T, Pizzorusso T. The roles of perineuronal nets and the perinodal extracellular matrix in neuronal function. Nature Reviews Neuroscience 2019;20:451–65.
[22] Paolicelli RC, Bolasco G, Pagani F, Maggi L, Scianni M, Panzanelli P, Giustetto M, Ferreira TA, Guiducci E, Dumas L, et al. Synaptic Pruning by Microglia Is Necessary for Normal Brain Development. Science 2011;333:1456–8.
[23] Pizzorusso T, Medini P, Berardi N, Chierzi S, Fawcett JW, Maffei L. Reactivation of Ocular Dominance Plasticity in the Adult Visual Cortex. Science 2002;298:1248–51.
[24] Rowlands D, Lensjo KK, Dinh T, Yang S, Andrews MR, Hafting T, Fyhn M, Fawcett JW, Dick G. Aggrecan Directs Extracellular Matrix-Mediated Neuronal Plasticity. J. Neurosci. 2018;38:10102–13.
[25] Shi W, Wei X, Wang X, Du S, Liu W, Song J, Wang Y. Perineuronal nets protect long-term memory by limiting activity-dependent inhibition from parvalbumin interneurons. Proceedings of the National Academy of Sciences 2019;116:27063–73.
[26] Thompson EH, Lensjø KK, Wigestrand MB, Malthe-Sørenssen A, Hafting T, Fyhn M. Removal of perineuronal nets disrupts recall of a remote fear memory. Proceedings of the National Academy of Sciences 2018;115:607–12.
[27] Blosa M, Sonntag M, Jäger C, Weigel S, Seeger J, Frischknecht R, Seidenbecher CI, Matthews RT, Arendt T, Rübsamen R, et al. The extracellular matrix molecule brevican is an integral component of the machinery mediating fast synaptic transmission at the calyx of Held. J. Physiol. (Lond.) 2015;593:4341–60.
[28] Gottschling C, Wegrzyn D, Denecke B, Faissner A. Elimination of the four extracellular matrix molecules tenascin-C, tenascin-R, brevican and neurocan alters the ratio of excitatory and inhibitory synapses. Sci Rep 2019;9:13939.
[29] Favuzzi E, Marques-Smith A, Deogracias R, Winterflood CM, Sánchez-Aguilera A, Mantoan L, Maeso P, Fernandes C, Ewers H, Rico B. Activity-Dependent Gating of Parvalbumin Interneuron Function by the Perineuronal Net Protein Brevican. Neuron 2017;95:639–55 e610.
[30] Hijazi S, Heistek TS, Scheltens P, Neumann U, Shimshek DR, Mansvelder HD, Smit AB, van Kesteren RE. Early restoration of parvalbumin interneuron activity prevents memory loss and network hyperexcitability in a mouse model of Alzheimer's disease. Molecular Psychiatry. 2019.
[31] Verret L, Mann EO, Hang GB, Barth AM, Cobos I, Ho K, Devidze N, Masliah E, Kreitzer AC, Mody I, et al. Inhibitory interneuron deficit links altered network activity and cognitive dysfunction in Alzheimer model. Cell 2012;149:708–21.
[32] Patel AR, Ritzel R, McCullough LD, Liu F. Microglia and ischemic stroke: a double-edged sword. Int J Physiol Pathophysiol Pharmacol 2013;5:73–90.
[33] Wen TH, Binder DK, Ethell IM, Razak KA. The Perineuronal 'Safety' Net? Perineuronal Net Abnormalities in Neurological Disorders. Front Mol Neurosci 2018;11.
[34] Rankin-Gee EK, McRae PA, Baranov E, Rogers S, Wandrey L, Porter BE. Perineuronal net degradation in epilepsy. Epilepsia 2015;56:1124–33.
[35] Franklin SL, Love S, Greene JR, Betmouni S. Loss of Perineuronal Net in ME7 Prion Disease. J. Neuropathol. Exp. Neurol. 2008;67:189–99.
[36] Crapser JD, Ochaba J, Soni N, Reidling JC, Thompson LM, Green KN. Microglial depletion prevents extracellular matrix changes and striatal volume reduction in a model of Huntington's disease. Brain 2019;143:266–88.
[37] Brückner G, Hausen D, Härtig W, Drlicek M, Arendt T, Brauer K. Cortical areas abundant in extracellular matrix chondroitin sulphate proteoglycans are less affected by cytoskeletal changes in Alzheimer's disease. Neuroscience 1999;92:791–805.
[38] Morawski M, Brückner G, Jäger C, Seeger G, Arendt T. Neurons associated with aggrecan-based perineuronal nets are protected against tau pathology in subcortical regions in Alzheimer's disease. Neuroscience 2010;169:1347–63.
[39] Miyata S, Nishimura Y, Nakashima T. Perineuronal nets protect against amyloid beta-protein neurotoxicity in cultured cortical neurons. Brain Res 2007;1150:200–6.
[40] Baig S, Wilcock GK, Love S. Loss of perineuronal net N-acetylgalactosamine in Alzheimer's disease. Acta Neuropathol. 2005;110:393–401.
[41] Cattaud V, Bezzina C, Rey CC, Lejards C, Dahan L, Verret L. Early disruption of parvalbumin expression and perineuronal nets in the hippocampus of the Tg2576 mouse model of Alzheimer's disease can be rescued by enriched environment. Neurobiol. Aging 2018;72:147–58.
[42] Morawski M, Brückner G, Jäger C, Seeger G, Matthews RT, Arendt T. Involvement of perineuronal and perisynaptic extracellular matrix in Alzheimer's disease neuropathology. Brain Pathol. 2012;22:547–61.
[43] Morawski M, Pavlica S, Seeger G, Grosche J, Kouznetsova E, Schliebs R, Brückner G, Arendt T. Perineuronal nets are largely unaffected in Alzheimer model Tg2576 mice. Neurobiol. Aging 2010;31:1254–6.
[44] Oakley H, Cole SL, Logan S, Maus E, Shao P, Craft J, Guillozet-Bongaarts A, Ohno M, Disterhoft J, Van Eldik L, et al. Intraneuronal β-Amyloid Aggregates, Neurodegeneration, and Neuron Loss in Transgenic Mice with Five Familial Alzheimer's

Disease Mutations: potential Factors in Amyloid Plaque Formation. The Journal of Neuroscience 2006;26:10129–40.
[45] Jawhar S, Trawicka A, Jenneckens C, Bayer TA, Wirths O. Motor deficits, neuron loss, and reduced anxiety coinciding with axonal degeneration and intraneuronal Aβ aggregation in the 5XFAD mouse model of Alzheimer's disease. Neurobiol. Aging 2012;33:196.e129–.
[46] Oddo S, Caccamo A, Shepherd JD, Murphy MP, Golde TE, Kayed R, Metherate R, Mattson MP, Akbari Y, LaFerla FM. Triple-transgenic model of Alzheimer's disease with plaques and tangles: intracellular Abeta and synaptic dysfunction. Neuron 2003;39:409–21.
[47] Hyman BT, Phelps CH, Beach TG, Bigio EH, Cairns NJ, Carrillo MC, Dickson DW, Duyckaerts C, Frosch MP, Masliah E, et al. National Institute on Aging-Alzheimer's Association guidelines for the neuropathologic assessment of Alzheimer's disease. Alzheimers Dement 2012;8:1–13.
[48] Tewari BP, Sontheimer H. Protocol to Quantitatively Assess the Structural Integrity of Perineuronal Nets ex vivo. Bio Protoc 2019;9:e3234.
[49] Buskila Y, Crowe SE, Ellis-Davies GCR. Synaptic deficits in layer 5 neurons precede overt structural decay in 5xFAD mice. Neuroscience 2013;254:152–9.
[50] Griciuc A, Patel S, Federico AN, Choi SH, Innes BJ, Oram MK, Cereghetti G, McGinty D, Anselmo A, Sadreyev RI, et al. TREM2 Acts Downstream of CD33 in Modulating Microglial Pathology in Alzheimer's Disease. Neuron 2019;103:820–35 e827.
[51] Keren-Shaul H, Spinrad A, Weiner A, Matcovitch-Natan O, Dvir-Szternfeld R, Ulland TK, David E, Baruch K, Lara-Astaiso D, Toth B, et al. A Unique Microglia Type Associated with Restricting Development of Alzheimer's Disease. Cell 2017;169:1276–90 e1217.
[52] Heneka MT, Carson MJ, Khoury JE, Landreth GE, Brosseron F, Feinstein DL, Jacobs AH, Wyss-Coray T, Vitorica J, Ransohoff RM, et al. Neuroinflammation in Alzheimer's disease. The Lancet Neurology 2015;14:388–405.
[53] Reed-Geaghan EG, Croxford AL, Becher B, Landreth GE. Plaque-associated myeloid cells derive from resident microglia in an Alzheimer's disease model. Journal of Experimental Medicine 2020;217.
[54] Pearson CS, Mencio CP, Barber AC, Martin KR, Geller HM. Identification of a critical sulfation in chondroitin that inhibits axonal regeneration. Elife 2018;7.
[55] Yi JH, Katagiri Y, Susarla B, Figge D, Symes AJ, Geller HM. Alterations in sulfated chondroitin glycosaminoglycans following controlled cortical impact injury in mice. J. Comp. Neurol. 2012;520:3295–313.
[56] DeWitt DA, Silver J, Canning DR, Perry G. Chondroitin Sulfate Proteoglycans Are Associated with the Lesions of Alzheimer's Disease. Exp. Neurol. 1993;121:149–52.
[57] Howell MD, Bailey LA, Cozart MA, Gannon BM, Gottschall PE. Hippocampal administration of chondroitinase ABC increases plaque-adjacent synaptic marker and diminishes amyloid burden in aged APPswe/PS1dE9 mice. Acta Neuropathol Commun 2015;3:54.
[58] Végh MJ, Heldring CM, Kamphuis W, Hijazi S, Timmerman AJ, Li KW, van Nierop P, Mansvelder HD, Hol EM, Smit AB, et al. Reducing hippocampal extracellular matrix reverses early memory deficits in a mouse model of Alzheimer's disease. Acta Neuropathol Commun 2014;2:76.
[59] Ali F, Baringer SL, Neal A, Choi EY, Kwan AC. Parvalbumin-Positive Neuron Loss and Amyloid-β Deposits in the Frontal Cortex of Alzheimer's Disease-Related Mice. Journal of Alzheimer's Disease 2019;72:1323–39.
[60] Saiz-Sanchez D, De La Rosa-Prieto C, Ubeda-Bañon I, Martinez-Marcos A. Interneurons and Beta-Amyloid in the Olfactory Bulb, Anterior Olfactory Nucleus and Olfactory Tubercle in APPxPS1 Transgenic Mice Model of Alzheimer's Disease. Anat. Rec. 2013;296:1413–23.
[61] Takahashi H, Brasnjevic I, Rutten BPF, Van Der Kolk N, Perl DP, Bouras C, Steinbusch HWM, Schmitz C, Hof PR, Dickstein DL. Hippocampal interneuron loss in an APP/PS1 double mutant mouse and in Alzheimer's disease. Brain Struct Funct 2010;214:145–60.
[62] Zallo F, Gardenal E, Verkhratsky A, Rodríguez JJ. Loss of calretinin and parvalbumin positive interneurones in the hippocampal CA1 of aged Alzheimer's disease mice. Neurosci. Lett. 2018;681:19–25.
[63] Balmer, T.S. (2016). Perineuronal Nets Enhance the Excitability of Fast-Spiking Neurons. eneuro 3, ENEURO.0112-0116.2016.
[64] Flanigan TJ, Xue Y, Kishan Rao S, Dhanushkodi A, McDonald MP. Abnormal vibrissa-related behavior and loss of barrel field inhibitory neurons in 5xFAD transgenics. Genes Brain Behav. 2014;13:488–500.
[65] Cabungcal JH, Steullet P, Morishita H, Kraftsik R, Cuenod M, Hensch TK, Do KQ. Perineuronal nets protect fast-spiking interneurons against oxidative stress. In: Proceedings of the National Academy of Sciences of the United States of America, 110; 2013. p. 9130–5.
[66] Tewari BP, Chaunsali L, Campbell SL, Patel DC, Goode AE, Sontheimer H. Perineuronal nets decrease membrane capacitance of peritumoral fast spiking interneurons in a model of epilepsy. Nat Commun 2018;9:4724.
[67] Lendvai D, Morawski M, Négyessy L, Gáti G, Jäger C, Baksa G, Glasz T, Attems J, Tanila H, Arendt T, et al. Neurochemical mapping of the human hippocampus reveals perisynaptic matrix around functional synapses in Alzheimer's disease. Acta Neuropathol. 2013;125:215–29.
[68] Kobayashi K, Emson PC, Mountjoy CQ. Vicia villosa lectin-positive neurones in human cerebral cortex. Loss in Alzheimer-type dementia. Brain Res. 1989;498:170–4.
[69] Virgintino D, Perissinotto D, Girolamo F, Mucignat MT, Montanini L, Errede M, Kaneiwa T, Yamada S, Sugahara K, Roncali L, et al. Differential distribution of aggrecan isoforms in perineuronal nets of the human cerebral cortex. J. Cell. Mol. Med. 2009;13:3151–73.
[70] Rogers SL, Rankin-Gee E, Risbud RM, Porter BE, Marsh ED. Normal Development of the Perineuronal Net in Humans; In Patients with and without Epilepsy. Neuroscience 2018;384:350–60.
[71] Kumar-Singh S, Cras P, Wang R, Kros JM, van Swieten J, Lübke U, Ceuterick C, Serneels S, Vennekens K, Timmermans JP, et al. Dense-core senile plaques in the Flemish variant of Alzheimer's disease are vasocentric. Am. J. Pathol. 2002;161:507–20.
[72] Wisniewski HM, Wen GY, Kim KS. Comparison of four staining methods on the detection of neuritic plaques. Acta Neuropathol. 1989;78:22–7.
[73] Mandrekar-Colucci S, Landreth GE. Microglia and inflammation in Alzheimer's disease. CNS Neurol Disord Drug Targets 2010;9:156–67.
[74] Serrano-Pozo A, Muzikansky A, Gómez-Isla T, Growdon JH, Betensky RA, Frosch MP, Hyman BT. Differential relationships of reactive astrocytes and microglia to fibrillar amyloid deposits in Alzheimer disease. J. Neuropathol. Exp. Neurol. 2013;72:462–71.
[75] Yin Z, Raj D, Saiepour N, Van Dam D, Brouwer N, Holtman IR, Eggen BJL, Möller T, Tamm JA, Abdourahman A, et al. Immune hyperreactivity of Aβ plaque-associated microglia in Alzheimer's disease. Neurobiol. Aging 2017;55:115–22.
[76] Najafi AR, Crapser J, Jiang S, Ng W, Mortazavi A, West BL, Green KN. A limited capacity for microglial repopulation in the adult brain. Glia 2018;66:2385–96.
[77] Dagher NN, Najafi AR, Kayala KM, Elmore MR, White TE, Medeiros R, West BL, Green KN. Colony-stimulating factor 1 receptor inhibition prevents microglial plaque association and improves cognition in 3xTg-AD mice. J Neuroinflammation 2015;12:139.
[78] Oddo S, Billings L, Kesslak JP, Cribbs DH, LaFerla FM. Abeta immunotherapy leads to clearance of early, but not late, hyperphosphorylated tau aggregates via the proteasome. Neuron 2004;43:321–32.
[79] Hong S, Beja-Glasser VF, Nfonoyim BM, Frouin A, Li S, Ramakrishnan S, Merry KM, Shi Q, Rosenthal A, Barres BA, et al. Complement and microglia mediate early synapse loss in Alzheimer mouse models. Science 2016;352:712–6.
[80] Geissler M, Gottschling C, Aguado A, Rauch U, Wetzel CH, Hatt H, Faissner A. Primary Hippocampal Neurons, Which Lack Four Crucial Extracellular Matrix Molecules, Display Abnormalities of Synaptic Structure and Function and Severe Deficits in Perineuronal Net Formation. The Journal of Neuroscience 2013;33:7742–55.
[81] Brakebusch C, Seidenbecher CI, Asztely F, Rauch U, Matthies H, Meyer H, Krug M, Böckers TM, Zhou X, Kreutz MR, et al. Brevican-Deficient Mice Display Impaired Hippocampal CA1 Long-Term Potentiation but Show No Obvious Deficits in Learning and Memory. Mol. Cell. Biol. 2002;22:7417–27.
[82] Bukalo O, Schachner M, Dityatev A. Modification of extracellular matrix by enzymatic removal of chondroitin sulfate and by lack of tenascin-R differentially affects several forms of synaptic plasticity in the hippocampus. Neuroscience 2001;104:359–69.
[83] Evers MR, Salmen B, Bukalo O, Rollenhagen A, Bösl MR, Morellini F, Bartsch U, Dityatev A, Schachner M. Impairment of L-type Ca2+Channel-Dependent Forms of Hippocampal Synaptic Plasticity in Mice Deficient in the Extracellular Matrix Glycoprotein Tenascin-C. The Journal of Neuroscience 2002;22:7177–94.
[84] Banerjee SB, Gutzeit VA, Baman J, Aoued HS, Doshi NK, Liu RC, Ressler KJ. Perineuronal Nets in the Adult Sensory Cortex Are Necessary for Fear Learning. Neuron 2017;95:169–79 e163.
[85] Gogolla N, Caroni P, Lüthi A, Herry C. Perineuronal Nets Protect Fear Memories from Erasure. Science 2009;325:1258–61.
[86] Tsien RY. Very long-term memories may be stored in the pattern of holes in the perineuronal net. Proceedings of the National Academy of Sciences 2013;110:12456–61.
[87] Romberg C, Yang S, Melani R, Andrews MR, Horner AE, Spillantini MG, Bussey TJ, Fawcett JW, Pizzorusso T, Saksida LM. Depletion of perineuronal nets enhances recognition memory and long-term depression in the perirhinal cortex. J. Neurosci. 2013;33:7057–65.
[88] Carulli D, Broersen R, de Winter F, Muir EM, Mešković M, de Waal M, de Vries S, Boele H-J, Canto CB, De Zeeuw CI, et al. Cerebellar plasticity and associative memories are controlled by perineuronal nets. In: Proceedings of the National Academy of Sciences, 117; 2020. p. 6855–65.
[89] Nguyen PT, Dorman LC, Pan S, Vainchtein ID, Han RT, Nakao-Inoue H, Taloma SE, Barron JJ, Molofsky AB, Kheirbek MA, et al. Microglial Remodeling of the Extracellular Matrix Promotes Synapse Plasticity. Cell. 2020.